Algal Research 36 (2018) 193–208

Contents lists available at ScienceDirect

Algal Research

journal homepage: www.elsevier.com/locate/algal

Potential of a liquid foam-bed photobioreactor for microalgae cultivation☆

Agnes Janoska[a,*], Vasilis Andriopoulos[a], Rene H. Wijffels[a,b], Marcel Janssen[a]

[a] AlgaePARC, Bioprocess Engineering, Wageningen University and Research, P.O. Box 16, 6700AA Wageningen, the Netherlands[1]
[b] Faculty of Biosciences and Aquaculture, Nord University, N-8049 Bodø, Norway

ARTICLE INFO

Keywords:
Microalgae
Photobioreactor
Foam-bed
Growth modeling
Energy requirement

ABSTRACT

The liquid foam-bed photobioreactor is a novel photobioreactor for microalgae cultivation. A mathematical model was developed to evaluate its potential, and to optimize the design and operation of a large-scale unit. This model describes light limited microalgal growth in a rising foam column in a foam-bed photobioreactor, which is continuously operated at constant biomass density. The microalgae-containing liquid is recirculated from the bottom of the reactor and dispersed equally on the top of the foam column, in order to ensure homogenous microalgae distribution and a wet and stable foam. The model combines calculations of liquid fraction gradient, light penetration, microalgal growth, and gas transfer in the foam-bed. The liquid fraction and light model was experimentally validated. The areal productivity of a 5 cm deep foam-bed photobioreactor operated at 30 g L^{-1} microalgae and 1500 µmol photons $m^{-2} s^{-1}$ was estimated to be 67.7 g $m^{-2} d^{-1}$. This productivity is slightly lower compared to what is achievable in flat panels, which is related to light scattering in the foam-bed. Nevertheless, the advantages of the foam-bed photobioreactor, such as high gas transfer rate and high biomass densities, were confirmed with the simulations. In addition, it was calculated that a CO_2 uptake efficiency of 97% can be obtained ensuring minimal CO_2 loss. These benefits result in reduced gas supply requirement and reduced energy required for downstream processing. The total energy required for the production and separation of 1 g biomass in liquid foam-beds is only 8.5% of what is required in flat panels with suspended biomass. These results highlight the potential of foam-bed photobioreactors for large scale application for microalgae production.

1. Introduction

In order to produce microalgal biomass at reduced costs and energy requirements, the importance of photobioreactor design has been highlighted in several studies [1–3]. A liquid foam-bed photobioreactor is an alternative photobioreactor concept to existing liquid-phase photobioreactors [4]. This reactor configuration was developed in order to reduce the energy requirements related to harvesting and gas supply. The reduction in harvesting costs is based on increased biomass densities due to the short light absorption length in the photobioreactor. The improved mass transfer is related to the increased surface area between the gas and the liquid phase, and the increased contact time between the CO_2-enriched gas and the microalgae-containing liquid. Additionally, reduced energy requirement for the gas supply is due to the reduced pressure drop in the reactor since the density of the foam is reduced compared to liquid. These presumed advantages, however, require exact characterization of the physical, chemical, and biological phenomena taking place in the reactor. Besides, in order to quantify the possible energy savings, the algal growth in the foam-bed photobioreactor has to be numerically evaluated. Therefore, a model predicting the productivity and energy requirements of a foam-bed photobioreactor was developed.

The operation of a foam-bed photobioreactor is based on continuous gas supply to a shallow layer of microalgae and surfactant containing solution. Due to the presence of surfactants, bubbles are formed, which will rise until the top of the reactor. In order to refresh the incorporated gas, the foam bubbles have to be broken. A possible method is to externally break the bubbles in a foam breaker device, as described for a previous foam-bed design [4]. Alternatively, the foam can be broken inside the reactor at the top. Due to the internal foam breaking the liquid fraction of the foam is enhanced as a result of the extra liquid drainage resulting from the liquid flux deliberated from broken bubbles [5]. A practically convenient solution is to break the foam with water jets. These water jets can originate from the microalgae-enriched liquid

☆ All authors agree to their authorship and to the submission of the manuscript to Algal Research for peer review.

* Corresponding author.
E-mail addresses: agi.janoska@gmail.com (A. Janoska), marcel.janssen@wur.nl (M. Janssen).

[1] www.wageningenur.nl/bpe, www.algaeparc.com and www.miraclesproject.eu.

https://doi.org/10.1016/j.algal.2018.09.029
Received 28 February 2018; Received in revised form 31 August 2018; Accepted 30 September 2018
2211-9264/ © 2018 The Authors. Published by Elsevier B.V. This is an open access article under the CC BY-NC-ND license (http://creativecommons.org/licenses/BY-NC-ND/4.0/).

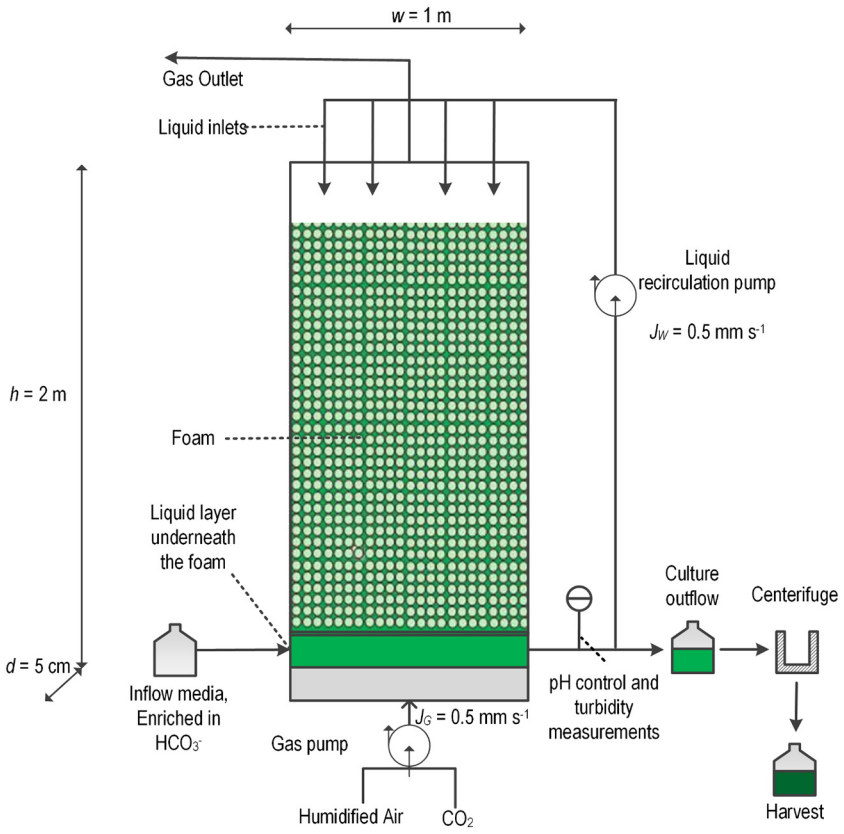

Fig. 1. Scheme of the liquid foam-bed photobioreactor modelled. The design of the foam-bed is improved compared to the previous design [4]: internal foam breaking and liquid recirculation have been introduced. The reactor dimensions and the gas and liquid recirculation flows indicated in Fig. 1 represent the baseline conditions during our simulations.

inside the reactor. Therefore, a liquid recirculation can be introduced, where the liquid from the bottom of the reactor is lead externally via pumps to the top where it is equally distributed over the foam column. This liquid drains down again in the foam column. Fig. 1 illustrates this improved foam-bed photobioreactor design including liquid recirculation and internal foam breaking. Due to the liquid recirculation and the internal foam breaking, the liquid fraction of the foam is enhanced. Enhanced liquid fraction in the foam is advantageous, since it produces a more stable foam [5], since both coalescence and coarsening are reduced [6,7]. In thin reactors or high light intensities, this elevated liquid fraction is also beneficial to absorb all incident light by increasing the light absorption path (i.e. more algae behind the 'window') resulting in increased productivity. The proof of principle of such a system has been confirmed at laboratory scale [8].

To create foam, Pluronic F68 was found to be a suitable surfactant in the liquid foam-bed photobioreactor. Despite its good foaming properties, lack of toxicity, and low biodegradability, microalgal partitioning to the foam phase formed by Pluronic F68 is reduced. Therefore, the microalgal concentration in the liquid content of the foam is lower compared to the liquid layer below the foam [9]. The liquid recirculation also circumvents this problem and ensures equal algal distribution in the foam, thereby resulting in an elevated microalgae concentration in the foam.

The model developed in this study describes a flat panel foam-bed photobioreactor with liquid recirculation and homogeneous liquid distribution on the top of the foam column. The reactor was operated in continuous mode: the biomass concentration does not change in time once a steady state is reached. The growth of a model microalgae strain, *Chlorella sorokiniana* was described. The developed model provides insight into the most important biological, chemical, and physical phenomena linked to the operation of foam-bed photobioreactors. The aim of the model is to determine the potential of the foam-bed photobioreactor and compare its potential productivity and energy requirement to conventional photobioreactors, e.g. flat panels. Next to that, the model aids further improvement in system design and operation. To achieve this, the influence of several operational parameters were investigated. Experimental validation took place for the core elements of the model (liquid fraction and light penetration).

2. Model structure, calculations, and assumptions

We modelled a flat panel photobioreactor filled with foam, under continuous illumination. The biological parameters were based on *Chlorella sorokiniana* CCAP 211/8k, a very productive species thoroughly studied in our laboratory [10]. A turbidostatic operational mode was considered. In practice, turbidity can be continuously measured in the liquid layer underneath the foam or in the recirculated liquid phase. The corresponding reactor dilution rates are equal to the algal specific growth rates, which depend again on the value of C_x. Time changes were irrelevant and therefore not considered in the mass balances used in this study. In the model we consider a constant pH of 6.7 throughout the whole foam column. In order to avoid CO_2 limitation, the required CO_2 concentrations were calculated and a constant gas flow rate was assumed.

In the simulations both design and operational parameters are varied in order to predict productivity and energy requirements of large scale foam-bed photobioreactors of different dimensions and under different operational conditions. The effect of biomass concentration, light levels, gas flow rate, liquid recirculation rate, bubble size, and reactor depth was determined on biomass productivity and operational energy requirements. As a baseline, a reactor of 2 m height, 1 m width and 5 cm depth was considered, operated under 1500 μmol m^{-2} s^{-1} incident light intensity, a biomass concentration of 30 g L^{-1}, a gas flow rate of 0.5 mm s^{-1}, and a liquid recirculation rate of 0.052 mm s^{-1}. Although a width of 1 m was considered to define a 'unit', the model aims to simulate a 1 m wide block of a large scale reactor with infinite width. The relevant reactor dimensions and gas and liquid recirculation flows are presented in Fig. 1. The applied values for the variables are

Table 1
Simulated design and operational conditions for the foam-bed photobioreactor.

Variable	Notation	Values			Unit
Biomass concentration	C_x	15	30	60	$g\,L^{-1}$
Light intensity	E_0	375	750	1500	$\mu mol\,m^{-2}\,s^{-1}$
Gas superficial velocity	J_G	0.05	0.5	2.5	$mm\,s^{-1}$
Liquid superficial velocity	J_w	0.026	0.052	0.104	$mm\,s^{-1}$
Bubble size	r_b	0.5	1	2	mm
Depth	d	0.01	0.5	0.1	m

presented in Table 1.

The model structure is presented in Fig. 2. Firstly the liquid fraction of the foam column is calculated as a function of height (ε). The liquid fraction profile is based on the physical-chemical properties of the liquid phase containing surfactant and microalgae, the gas flow rate, and the liquid recirculation flow rate. Most existing models describing foam-bed reactors do not consider the liquid fraction gradient, but assume a constant liquid fraction in height [11]. The description of this gradient in this study allows for more precise calculations. This liquid fraction profile influences the optical properties of the foam at different heights: at higher liquid fractions more microalgae are present, and also the scattering properties of the foam will be influenced. Based on the optical properties of the foam, the local light availability inside the foam-bed can be predicted. The light penetration in the foam was modelled with the light diffusion theory. The foam has a highly scattering nature, thus at a certain position in the foam photons are arriving from all directions: in this case we talk about fluence rate (ϕ), owing the same units as irradiance [Wm^{-2} or μmol photons $m^{-2}\,s^{-1}$]. From the local fluence rate availability, the microalgae growth rate (μ), the resulting biomass productivities (volumetric and areal productivity, r_x and r_x^{Areal}, respectively) and biomass yield on light ($Y_{x,ph}$) were calculated. The biomass production rate determines the CO_2 requirements for the algal growth. With the gas transfer model, the minimal CO_2 concentration that should be supplied within the inlet gas phase ($C_{CO2}^{G,in}$) could be predicted. From the inlet and outlet CO_2 concentrations the CO_2 uptake efficiency, η_{CO2} could be determined. In addition, the O_2 accumulation in the liquid phase (C_{O2}^{L}) could be calculated. The operational energy requirements (E) were then calculated based on the energy requirements for gas supply by gas blowers, liquid recirculation by liquid pumps, and biomass separation by centrifuges.

In the model, the following assumptions were applied:

- The bubbles are spherical, with uniform size (no expansion in height due to pressure differences or due to gas diffusion, no coalescence/coarsening/breakage). A decreasing liquid fraction therefore means an increasing number of gas bubbles in a given volume.
- The distribution of the recirculated liquid on the top of the foam column is homogenous.
- The liquid phase is ideally mixed. Most previous mass transfer

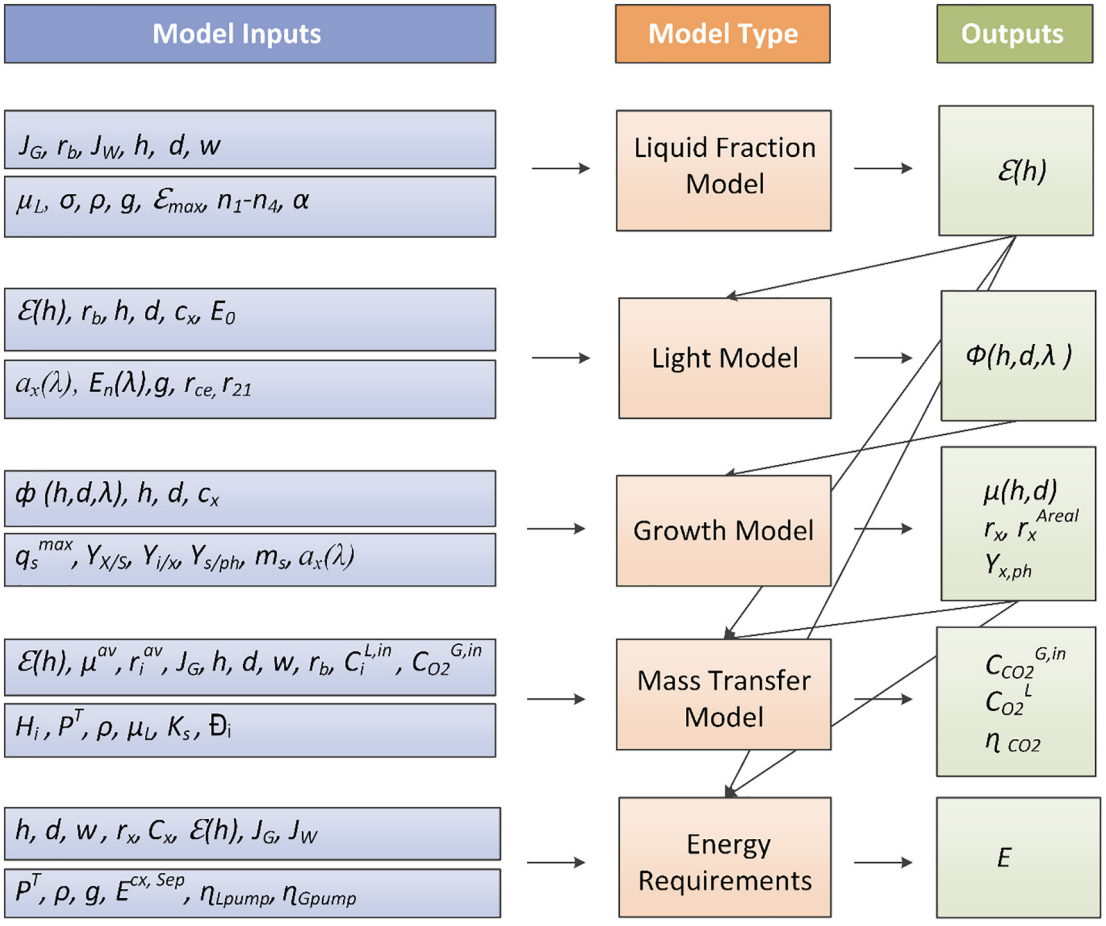

Fig. 2. Scheme of the model describing the performance of foam-bed photobioreactors. The left column (blue rectangles) shows the model inputs, which are used to calculate the model outputs listed in the right column (green rectangles). The model outputs include liquid fraction as a function of height, ε(*h*); fluence rate distribution, ϕ(*h*,*d*,λ); local growth rates, μ(*h*,*d*); volumetric and areal biomass productivities, r_x and r_x^{Areal}, respectively; biomass yield on light $Y_{x,ph}$, inlet CO_2 concentration, $C_{CO2}^{G,in}$; O_2 concentration in the liquid phase C_{O2}^{L}; CO_2 uptake efficiency (η_{CO2}) and biomass specific energy requirements, *E*. Explanation of model inputs can be found in the Supplementary Information. (For interpretation of the references to colour in this figure legend, the reader is referred to the web version of this article.)

models on foam-reactors assume stagnant liquid layers, where mass transfer is solely via diffusion [11,12]. This is because limited mixing took place in these reactors since liquid recirculation was not applied. In case of foam reactors with liquid recirculation, an ideally mixed liquid phase was reported previously [13]. This assumption is further supported by the reduced retention time of recirculated the liquid compared to gas phase of the foam-bed.

- The gas phase within each gas bubble is ideally mixed, similarly with previous foam-bed models [12], but individual gas bubbles do not interact.
- The liquid layer underneath the foam column has negligible volume. Therefore no gas transfer and no growth take place in this area. This assumption is made since in practice, the volume of this liquid layer is minimized.
- Liquid phase density, surface tension, viscosity were measured once for a specific biomass density and assumed to be constant for the different simulations with different biomass densities.
- The gas phase resistance is negligible, therefore only liquid phase gas transfer resistance (k_L) is considered.
- Henry's law is applied for the dissolution of oxygen and carbon dioxide. We thus assume dilute solutions at low partial pressures. Solubility of oxygen and carbon dioxide is not corrected for increased ionic strength.
- Absolute pressure is assumed to be 1 atm at each position in the foam-bed, since the hydrostatic pressure of the foam column simulated causes < 2% deviation from the atmospheric pressure.
- All gases behave as ideal gases.
- No loss of H_2O by evaporation takes place because the gas is humidified before entering the foam-bed.
- No change in pH occurs across the foam-bed.
- Light escaping from the foam reactor top or bottom is neglected.

2.1. Liquid fraction gradient in foams

The liquid fraction is an important parameter of foams, determined by surfactant type and concentration, gas flow rate, design of gas distributor, and further physical-chemical properties of both the foamed solution (density, viscosity, surface tension) and of the formed foams (bubble size, rigidity of interfaces and dispersity of bubble size distribution) [14]. It is well known that the liquid fraction in rising foams is not constant: at the bottom, at the point of foam generation wet foam is present, while at the top, the foam is drier because of drainage of the liquid [5]. The visual differences between wet and dry foam in a rising foam column can be seen in Fig. 3.

The liquid fraction gradient in height in a rising foam can be calculated according to Yazhgur et al. [14]. In case additional liquid is supplied to the top of the foam column, the liquid fraction of the foam is elevated due to the drainage of the supplied liquid through the foam-bed. To account for this, the theory of Yazhgur et al. can be supplemented by Stevenson's concept about liquid addition from the top [5].

The theory of Yazhgur is based on the calculation of the net superficial liquid velocity in rising foams, which can be obtained from the sum of the upward liquid movements and the relative downward liquid movements. The net superficial liquid velocity is constant through the foam-bed due to the conservation of mass. The upward liquid flux is caused by gas bubbles rising and dragging liquid along upwards. However, the liquid does not travel at the same speed as the gas bubbles due to drainage. This drainage is caused by gravity but also counteracted by capillary forces originating from the osmotic pressure gradient in height. This osmotic pressure is created by the difference between the energetic states of the interfilms originating from the varying bubble sphericity, which is determined by the liquid fraction of foams. Consequently, liquid drainage through the foam depends on liquid fraction gradient.

In a rising foam, the net liquid superficial velocity (J_f) owns an upward direction since the foam volume is continuously increasing and the volume of the liquid on the bottom used to form foam is thus decreasing. In case of additional liquid supply to the top of the foam column, the net liquid superficial velocity might change orientation. Considering continuous foam breaking at a given height, the water liberated from the broken bubbles can be seen as an additional liquid flux. Thus, the net liquid superficial velocity when foam breaking is applied will be 0, since the water addition rate resulting from foam breaking (J_w^{fb}) equals to the net upward superficial velocity of a rising foam without foam breaking. In case both foam breaking and external liquid recirculation is applied, the net superficial velocity will be orientated downwards, and its value will equal to the water addition rate, $J_f^{w+fb} = -J_w$.

Fig. 3. Liquid fraction gradient in a rising foam column, without applying liquid recirculation. The liquid fraction of the foam is high at the bottom of the foam column, close to the foam-liquid interface, while it is decreasing towards the top foam layers.

By knowing the steady state net liquid superficial velocity of the foam, the liquid fraction gradient in height of the foam can be expressed with the upward and downward liquid fluxes. A mathematical description of this theory can be found in the Supplementary Information.

2.2. Light penetration in foams

When a collimated beam perpendicularly hits the reactor surface, part of the light is reflected at the surface, while the remaining collimated light is attenuated in the foam-bed by algal absorption and scattering by the foam structure itself (caused by multiple reflections at the bubble liquid interface). By multiple scattering events, diffuse light is generated. Therefore, light propagation in the foam-bed photobioreactor was modelled assuming light diffusion theory, which is required due to the highly scattering nature of the foam. Consequently, the algal cells in the foam-bed do not only receive light from a single direction but photons can arrive from each possible direction. In this case we talk about fluence rate, owing the same units as irradiance [Wm^{-2} or $\mu mol\,photons\,m^{-2}\,s^{-1}$]. Diffusion theory is a relatively simple method to model light propagation in a scattering medium although the accuracy of diffusion theory is reduced close to the system boundaries and the light source, and in situations where strong absorption takes place compared to scattering [15].

The path of collimated light is indicated with yellow arrows in Fig. 4. The attenuation of collimated light due to scattering and absorption is modelled based on Lambert Beers law. The diffuse light generated also attenuates in forward and backward directions due to further absorption and scattering as indicated with orange arrows in Fig. 4. Both the collimated and diffuse light are partly reflected at the transparent reactor sides. In this study a reactor with glass walls was considered, therefore reflections at air-glass and glass-liquid interfaces

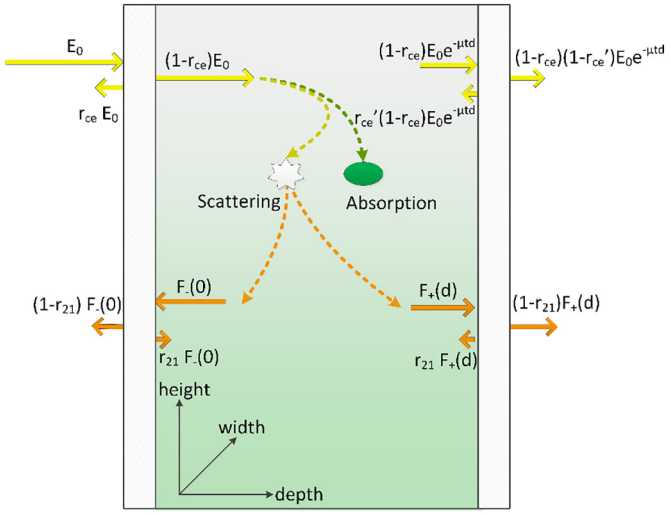

Fig. 4. Light propagation in a liquid foam-bed. The incident collimated light beam is partially reflected at the surface of the reactor (yellow arrows indicate collimated light). Collimated light transmitted through the reactor wall is absorbed and scattered inside the foam and, consequently, it results in diffuse light going in forward and backward directions (indicated by orange arrows). Both the collimated and the diffuse light inside the foam is partially reflected at the surface of the reactor before a light beam leaves the reactor. (For interpretation of the references to colour in this figure legend, the reader is referred to the web version of this article.)

were taken into account.

The fluence rate can be predicted at each point in the reactor when knowing the reflection factors for both diffuse and collimated light at the reactor sides and the scattering and absorption coefficients of the foam with microalgae. The latter two are dependent on the liquid fraction, and thus on the height in the reactor. The scattering coefficient is further influenced by the foam bubble size, and the absorption coefficient is determined by the biomass concentration and the wavelength specific absorption cross section of the microalgal biomass. Scattering by the algal cells is not included in the model. For the simplicity of the light model, we did not consider the interaction of scattered light originating from different heights with different optical properties. Thus, the fluence rate at a certain height is only dependent on the liquid fraction at that given height and not on the liquid fraction in the layers below and above. This assumption proved to be acceptable because the calculated liquid fraction was constant over the largest part of the height. The liquid fraction was higher only over a few centimetres above the liquid level where foam is generated. Additionally the validity of light transport equations used in this study was confirmed by additional simulations using the diffusion approximation [15], which takes into account both the horizontal and vertical light spreading. The fluence rate distribution showed a perfect match with the diffusion approximation simulations under the simulation conditions, which might be reasoned by that when high biomass concentrations are applied and absorption increases, the influence of scattering from other layers is reduced.

The theory for light propagation in an infinitely wide and high, but finitely thick slab (in depth), illuminated by wide-beam collimated light is considered [15]. The depth is defined in the direction of the incident collimated light beam. Since the reactor height is fixed at 2 m, edge effects taking place near the reactor top and bottom are neglected. There are no boundaries at reactor sides which are parallel to the incoming light since a 1 m wide element of an infinitely wide reactor is considered in our simulations. The light model developed in this study is mathematically explained in the Supplementary Information. It predicts the fluence rate in the reactor at any position (thus at given height and depth coordinates) accounting for the spectral distribution of the incident light and also the spectral distribution of the absorption coefficient of the microalgal cells for wavelengths between 400 and 700 nm (wavelength specific values are presented in the Supplementary Information).

2.3. Microalgae growth model

The microalgae specific growth rate inside a liquid foam-bed photobioreactor was modelled based on the local fluence rate. For the growth, nitrogen is supplied in the form of urea. Algal growth is modelled according to Jassby & Platt's model, where the algal growth rate is related to its sugar production rate, which is defined by the light availability [10]. The local fluence rates are determined by the previously described light model and it includes all photons within the photosynthetically active radiation (PAR) range, ranging from 400 to 700 nm. Above a certain light intensity (or fluence rate), which is called the light saturation point, excess light is dissipated by the algal cells. At fluence rates below the light saturation point the microalgae specific growth rate is proportional to the fluence rate. Although mixing times in the foam-bed photobioreactor are in the order of several minutes, this is still considerably smaller than the characteristic time of photoacclimation which is in the order of hours. Photoacclimation can thus be neglected and a constant wavelengths-specific value is used for the microalgae-specific light absorption cross section, a_x. The value of a_x was determined assuming a mass culture acclimated algal cell.

The local specific growth rates were averaged over the complete liquid volume of the foam-bed due to the assumption of an ideally mixed liquid phase. The resulting average specific growth rate is used to calculate the volumetric biomass production rate, areal productivity defined as biomass production rate per unit of illuminated surface area, and biomass yield on light. The volumetric biomass production rate determines the O_2 production and CO_2 consumption rates. The corresponding equations are presented in the Supplementary Information.

2.4. Gas transfer model

The gas transfer in the foam is modelled by assuming an ideally mixed liquid phase, while the gas phase moves upwards in plug-flow (Fig. 5). The plug flow behaviour of the gas was based on the fact that the gas bubbles are physically separated, so a gradient in height will occur. This gradient is characterised by a decreasing CO_2 concentration and an increasing O_2 concentration with height due to the transfer between gas bubbles and liquid with photosynthesising algae. An ideally mixed liquid phase is a simplification but is based on the calculation that the residence time of the recirculated liquid in the foam-bed is at least 3 times smaller than that of the gas phase (calculation based on model results presented later). This assumption is further supported by previous reports on a well-mixed zone in the foam below the liquid addition level [13]. Consequently, the liquid phase concentration of a certain compound is constant everywhere (no dependence on y and z) whereas the liquid fraction $\varepsilon(y)$, the gas phase concentrations $C_i^G(y)$ and the transfer coefficients $k_La(y)$ are dependent on the height of the reactor.

In the model calculations only the liquid phase mass transfer resistance was considered and the gas side limitations were neglected. The volumetric mass transfer coefficient, k_La [s^{-1}], was calculated from the liquid side mass transfer coefficient $k_L(y)$ and the surface area available for mass transfer per unit volume of foam, $a(y)$, which are both dependent on the liquid fraction of the foam. The $k_L(y)$ is calculated by a correlation for a packed-bed of solid spheres, which provides a good match with the $k_L(y)$ of foam-beds [16]. This correlation is based on the difference between gas and liquid velocities, determining the Reynolds number, and further dimensionless numbers (Schmidt and Sherwood numbers) related to diffusion coefficient, liquid phase properties and bubble size [16].

In order to avoid CO_2 limitation and ensure light limited growth, the

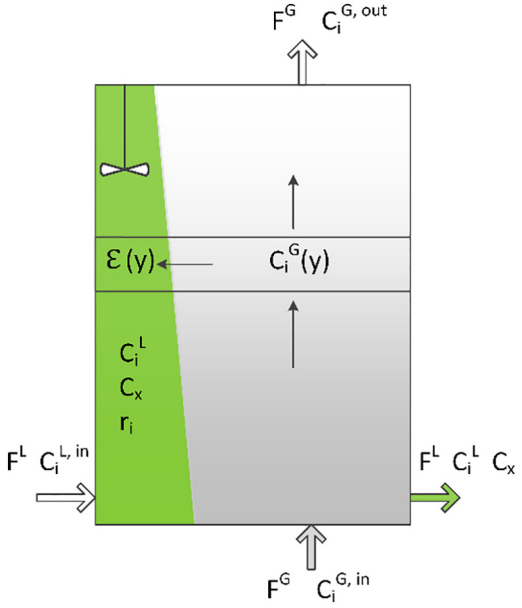

Fig. 5. The gas transfer model of the foam-bed photobioreactor. The foam is modelled as a separate liquid and gas phase, with the interfacial area in between them related to the surface area of the bubbles at different heights. The decrease of the liquid fraction in height was modelled as an increase in the number of gas bubbles compared to liquid volume. The liquid phase was assumed to be ideally mixed while the gas moves upwards in plug-flow.

overall $C_{CO2}{}^{L}$ needs to be sufficiently high. This limit is arbitrarily set at $5{\cdot}K_s$, where K_s is the CO_2 concentration where the growth rate is decreased to half of its maximal value. Thus, a minimum $CO_2{}^{G}(in)$ concentration in the inflow gas has to be determined that results in $C_{CO2}{}^{L} \geq 5{\cdot}Ks$. With this given liquid CO_2 concentration, the CO_2 concentration required in the inlet gas can be calculated from a combination of mass balances and consequently the CO_2 uptake efficiency can also be expressed. In the continuous liquid inflow, $HCO_3{}^{-}$ is supplied at a concentration of $5{\cdot}Ks$. The liquid O_2 concentration can be determined as well by the given inlet gas composition and the microalgal O_2 production rate. In case of oxygen accumulation in the liquid phase, oxygen inhibition might take place [17] but this inhibition is not included in the model. The corresponding model equations are included in the Supplementary Information.

2.5. Energy requirements

The energy requirements for a foam-bed photobioreactor were calculated considering gas supply, liquid recirculation, and harvesting. The energy requirements for the gas supply by gas blowers or compressors were determined based on adiabatic compression of the gas. The pressure of the compressed gas has to equal to the hydrostatic pressure of the water column. An efficiency of 70% was applied as described for a rotary compressor [18]. For pumping liquid to higher levels the hydrostatic pressure and the volumetric recirculation flow rate was considered. The pump efficiency depends on pump design, and in this study an efficiency of 75% was used according to Ruiz et al. [2]. The energy requirement for the algal separation are determined by the biomass concentration and the method of harvesting. We considered harvesting by centrifugation and assumed a plate separator (or disk centrifuge) requiring 1.5 kWh ($5.4{\cdot}10^6$ J) per 1 m^3 of algal suspension to be separated [19].

3. Materials and methods

3.1. Parameter determination

The viscosity of M8a media, surfactant solution (10 CMC Pluronic F68 corresponding to 3.34 $g\,L^{-1}$), and microalgae cultures (*Chlorella sorokiniana*) prepared in M8a media with and without surfactant were measured with Ubbelohde viscometers. The Pluronic F68 surfactant was obtained from Panreac Applichem (Spain). The calibration of the viscometer was done by glycerol solutions of known viscosities. The experiments were done at room temperature, ensured with submerging the viscometers in a water bath (21.5–22 °C). The viscosity of a solution containing 5 $g\,L^{-1}$ *Chlorella sorokiniana* was applied in the model.

The surface tension of the above mentioned solutions were measured with a drop tensiometer, analysing the shape of a hanging drop (Teclis Tracker). In these experiments a microalgae concentration of 7.8 $g\,L^{-1}$ was used.

3.1.1. Model implementation in Matlab

For the model simulations the reactor was divided into 400 depth and 100 height segments. The liquid fraction gradient in height was determined by a differential equation solver (ODE45), while the gas concentrations were determined by manual integration, thus the stepwise changes in height were implemented, according to Eq. (1). The accuracy and convergence of the numerical integration with the method presented in Eq. (1) was confirmed by additional simulations at increased number of steps.

$$X(h + \Delta h) = X(h) + \Delta h{\cdot}f(h) \quad (1)$$

where X indicates the variable at a certain height, Δh is the height step, and f is the function describing the differential dx/dh. Light and growth model results were expressed in terms of horizontal and vertical position and also as a function of wavelength, therefore the output was expressed in a 3D matrix. For further calculations, growth rates and production rates were summed for all wavelengths and were averaged over the liquid volume in the foam-bed. The detailed equations are presented in the Supplementary Information. Optimization of the liquid recirculation rate was done applying the Global Optimization Toolbox, GlobalSearch optimization solver. For the simulation, the following data was applied: $C_x = 30\,g\,L^{-1}$, $r_b = 1$ mm, $J_G = 0.5\,mm\,s^{-1}$, $J_w = 0.052\,mm\,s^{-1}$, $E_0 = 1500\,\mu mol\,m^{-2}\,s^{-1}$, $d = 5$ cm. The wavelength dependence was taken into account both for the absorption cross section and for the irradiance.

3.1.2. Experimental model validation: liquid fraction of foam-beds

In order to determine the liquid faction of Pluronic F68 foams, experiments were carried out in an automatized Foamscan (Teclis- IT Concept, Logessaigne, France). Experiments were performed at varying column height (20.79 and 14.15 cm), gas flow rates (0, 2.36 and 4.46 $mm\,s^{-1}$), and liquid addition rates (0, 0.092 and 0.36 $mm\,s^{-1}$). Foam was generated in a glass cylinder by blowing nitrogen gas through a metal frit with small conical holes (30 μm and 100 μm hole diameter on the top and the bottom of the cone, respectively). The smaller cylinder corresponding to the lower column height has a diameter of 3.5 cm, and 40 mL solution was used for foam formation, while in the bigger cylinder (diameter of 6 cm) 60 mL solution was used. After the foam volume has reached 400 cm^3, or 200 cm^3 in the small column, the gas flow automatically stopped. In case of liquid addition, the foam was left for ~10 min to drain and thus a dry foam was achieved before the liquid addition was initiated. The evolution of the bubble sizes was monitored by image analysis at a height of 8 cm above the gas distributor. The bubble size was calculated by image analysis software (Foamscan). The temperature of the glass cylinder was between 24 and 30 °C in all experiments. The surfactant concentration applied was 5 or 10 CMC. The experiments were performed in duplicate. The liquid fraction of the foam was determined from conductimetric analysis of

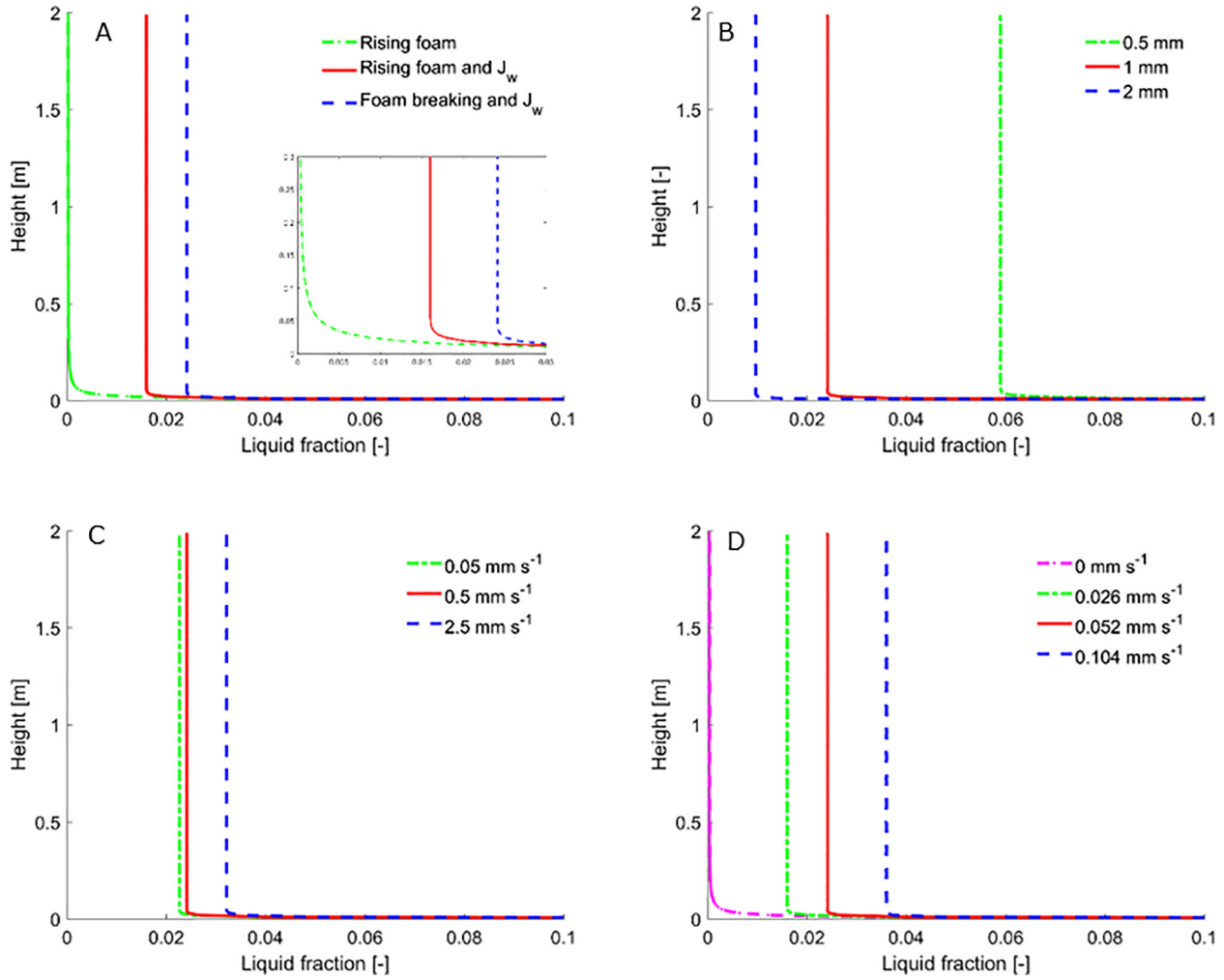

Fig. 6. Liquid fraction of foams as a function of height in the foam-bed. (a) Liquid fraction of a rising foam, a rising foam with liquid recirculation, and a foam which is broken at the top with additional liquid recirculation. The insert is zoomed in to the same image. (b) Liquid fraction at varying bubble radius r_b; (c) Liquid fraction at varying superficial gas flow rate J_G; (d) Liquid fraction at varying superficial liquid recirculation rates J_w. For the simulation, the following inputs were applied: $r_b = 1$ mm, $J_G = 0.5\,\mathrm{mm\,s^{-1}}$, $J_w = 0.052\,\mathrm{mm\,s^{-1}}$, $h = 2$ m with foam breaking at the top.

the liquid volume of the solution remaining on the bottom of the cylinder. The total liquid fraction of the foam is calculated by dividing the volume of liquid incorporated in the foam by the foam volume.

When liquid addition was applied, the average liquid fraction over the whole column was calculated by Eq. (2).

$$\varepsilon = \frac{J_d}{v_{wetfront}} \tag{2}$$

where J_d is the superficial liquid flow rate from the top (the liquid addition rate), and $v_{wetfront}$ is the measured liquid velocity. Thus, since the drainage only occurs via the liquid phase of the foam, not over the whole cross-sectional area, the liquid fraction can be calculated. The wet front velocity was determined by measuring the time required for the liquid added from the top to arrive to the bottom of the foaming column, and this time was divided by the height of the foam column. The moment when the wet front arrived at the bottom of the column was indicated by increase in the liquid volume, which was determined by conductivity measurements. Since only the time point was required when the wet front arrived at the bottom of the foam column, there was no need for continuous operation.

3.1.3. Experimental model validation: light penetration in foam

In order to determine the light distribution in liquid foams, fluence rate measurements were carried out at several points in depth, inside a liquid foam-bed. Fluence rate was determined by submerging a spherical light sensor (Walz, US-SQS/A) into absorbing and non-absorbing foams. Foam formation took place by distributing gas in a surfactant containing solution in a glass container of 20.5·3·40 cm (width × depth × height). The gas was distributed via a silicon tube (4 mm inner diameter, 2 mm wall thickness) punched with a 0.45 mm needle every 1.4 cm. Foams were formed by Pluronic F68 at a concentration of 2 CMC in a 350 mL initial solution. The liquid solution was recirculated from the liquid layer underneath the foam to the top of the foam column by peristaltic pumps and was distributed at 4 different points at the top of the foam column. This resulted in a superficial liquid flow rate of $0.27\,\mathrm{mm\,s^{-1}}$. Foams were formed at a superficial gas low rate of $2.78\,\mathrm{mm\,s^{-1}}$, but during the measurements the gas distribution was temporarily stopped.

Fluence rate measurements were done at 0, 3, 19, 27 and 30 mm from the vertical light exposed surface, at a height of 25 cm and in the middle of the reactor width (10.25 cm from both sides). The light source was composed of 20 circular warm-white LED lamps (Bridgelux, BXRA W1200, Bridgelux, USA) equipped with 42 mm diameter Brooke-S (spot) reflector (LEDIL F'FORM OPTICS, Finland). The upper 31 cm of the glass tank was irradiated with $475\,\mu\mathrm{mol\,m^{-2}\,s^{-1}}$. A distance of 47 cm was kept between the reactor and the light source to ensure homogenous light distribution on the flat glass tank. Measurements were done in foams without microalgae (clear foam), and at 0.6, 2.6

and 6 g L^{-1} *C. sorokiniana* concentration. The reflected and transmitted flux from the glass tank was measured with a flat 2π PAR quantum sensor (LI-SA-190, LI-COR, USA). The transmitted flux was measured directly behind the glass tank, while the reflected flux was measured on the light source, 45.5 cm from the glass tank, in between the LED lamps to prevent shading. The measured reflected flux was expressed relative to the reflected flux from white paper (3 sheets of 80 g m^{-2}) which was placed at the location of the glass tank. The reflected flux from the white paper sheets was assumed to represent ideal diffuse reflectance. The values were further corrected for residual ambient light by subtracting the reflected flux in case of black paper placed at the location of the glass reactor, which represents complete absorbance. The bubble size of the foam in the vessel was determined manually by image analysis, where 120 bubbles were measured.

4. Results

4.1. Liquid fraction in a foam-bed photobioreactor

The liquid fraction gradient in the foam was modelled for three cases: a) continuously rising foam-bed; b) continuously rising foam-bed with liquid addition from the top; c) rising foam-bed which is broken at a certain height with liquid addition from the top.

Generally, the liquid fraction of foams decreases quickly with height. The maximum liquid fraction at the bottom of the foam column is 0.26 in case of ordered foams with homogenous bubble size distribution. The model results show (Fig. 6A) that by liquid addition, the liquid fraction of rising foam can be increased because of continuous drainage of the added water through the foam structure. When the rising foam is continuously broken, the liquid fraction is further elevated since foam breaking can be regarded as external liquid addition. By applying liquid addition or foam breaking, the liquid fraction profile is more homogenous (or 'flat') compared to the liquid fraction profile of rising foams (See Fig. 6A, insert). This flat profile is advantageous in order to create a similar horizontal light gradient along the foam column. The simulated liquid fraction profiles correspond well to the profiles reported by P. Stevenson [5].

Additional simulations showed that higher liquid addition rates (J_w), smaller bubbles (r_b), and higher gas flow rates (J_G) lead to increased liquid fraction of the foam (Fig. 6B, C, D). In order to create wet foams, liquid addition is the best way, since the gas flow rates and foam breaking in the absence of additional liquid supply have minor effect on liquid fractions compared to liquid recirculation. Decreasing bubble size also significantly increases the liquid fraction of foams. However, this would require altered gas distributer design or increased surfactant concentrations. Experiments to obtain model parameters and experiments to partly validate the model are presented in the Appendix.

4.2. Light profile in a foam-bed photobioreactor

The fluence rate inside the photobioreactor is influenced by the biomass concentration (C_x), bubble size (r_b), the illuminating light intensity (E_0) and the liquid fraction of the foam (ε). The liquid fraction, as demonstrated before, is dependent again on both the superficial gas velocity (J_G) and the superficial liquid recirculation velocity (J_w). The fluence rate is linearly proportional to E_0 (see Supplementary Information) and also reflectance and transmittance are linearly proportional to E_0.

On the bottom of the reactor, close to the height of foam generation the foam has a high liquid fraction, resulting in lower fluence rate compared to the top of the foam (Fig. 7A). At the front of the reactor, the fluence rate can be higher than the incident irradiance (Fig. 7) because of photons arriving to this layer from both forward and backward direction due to light scattering. This light profile is less advantageous for algae growth because of a relative increase in light saturation at the light exposed surface, and also because of a deeper points towards the back of the reactor, the light availability is decreased.

In non-absorbing foams (C_x = 0 g L^{-1}), the fluence rate peaks at approximately 1 cm deep in the reactor, afterwards it steeply decreases with depth (Fig. 7B). At higher biomass concentrations, the fluence rate at the reactor front approaches the incident light intensity and decreases exponentially from the start (the peak is absent) due to both absorption and scattering (Fig. 7B). With increasing biomass concentration, both the transmitted light and reflected light decreases due to the stronger absorption (Table 2).

By varying the liquid fraction of foams by varying liquid recirculation (J_w), both scattering and absorbing behaviour of the foam changes. At low liquid fractions, light absorption is reduced due to the reduced amount of microalgae present, but also light scattering is reduced since the scattering coefficient is influenced by the liquid fraction (See Supplementary Information). On the one hand, because of reduced light absorption the fluence rate has a higher initial value and the light gradient is less steep at lower liquid fractions (Fig. 7C). Also the elevated reflectance and transmittance at low liquid fractions (Table 2) is explained by the relative decrease in absorption. On the other hand the effect of scattering is also influential and it becomes clear when equal absorption is ensured in absorbing foams with different liquid fractions, achieved by compensating for the reduced liquid fractions with elevated biomass concentrations. The case of reduced liquid fraction and increased biomass concentration enables deeper light penetration in the reactor due to a less steep light attenuation, therefore in this case a more advantageous light profile can be achieved.

Increased gas flow rates and decreased bubble sizes also result in increased liquid fraction, therefore similar light profiles are achieved as when increasing the liquid recirculation rate. Bubble radius, however, does not only influence the liquid fraction, but also affects the scattering coefficient. Larger bubble sizes reduce the extent of scattering also when the liquid fraction is kept constant (e.g. by adjusting J_w). Therefore, the combined effect of large bubbles on both liquid fraction and scattering result in lower fluence rates at the reactor front and a less steep decrease of fluence rate with depth compared to smaller bubbles (Fig. 6D). Accordingly, reflectance is decreased and transmittance is increased compared to smaller bubbles (Table 2).

4.3. Gas transfer

The gas transfer rate in the liquid foam-bed photobioreactor was modelled and used to calculate the gas transfer capacity and efficiency. First, the biomass production rate was calculated according to the growth model based on the local fluence rates. The biomass production rate was 53.3 g L_{liquid}^{-1} d^{-1} under the following conditions: C_x = 30 g L^{-1}, d = 5 cm, h = 2 m, E_0 = 1500 μmol m^{-2} s^{-1}, J_w = 0.052 mm s^{-1}, J_G = 0.5 mm s^{-1}. This biomass production rate determines the CO_2 requirement of the growing algal culture. The gas transfer model was then used to calculate the carbon dioxide (CO_2) supply rate preventing CO_2 limitation in the foam-bed photobioreactor. More specifically, the minimal inlet CO_2 fraction was calculated when a constant superficial gas velocity was applied. It was calculated that at fixed 0.5 mm s^{-1} superficial gas velocity, 6.9% CO_2 is required (Fig. 8A) in order to maintain the liquid phase CO_2 concentration at 5·K_s at the above mentioned conditions. The outgoing CO_2 concentration in the gas phase is approaching 0.2%, therefore a CO_2 uptake efficiency of 97% can be obtained, and negligible CO_2 is lost. As a comparison, in the most efficient conventional photobioreactors, thin-layered liquid phase photobioreactors [20], flat-panel airlift photobioreactors [21], or tubular photobioreactors [22], > 50% of the CO_2 is not taken up and lost to the environment. It must be noted that also in these conventional photobioreactors very high CO_2 uptake efficiencies can be reached by adapting operation and design (for example gas recirculation). Such maximization of CO_2 uptake efficiency, however, goes at the expense of reduced productivity and/or increased energy demand.

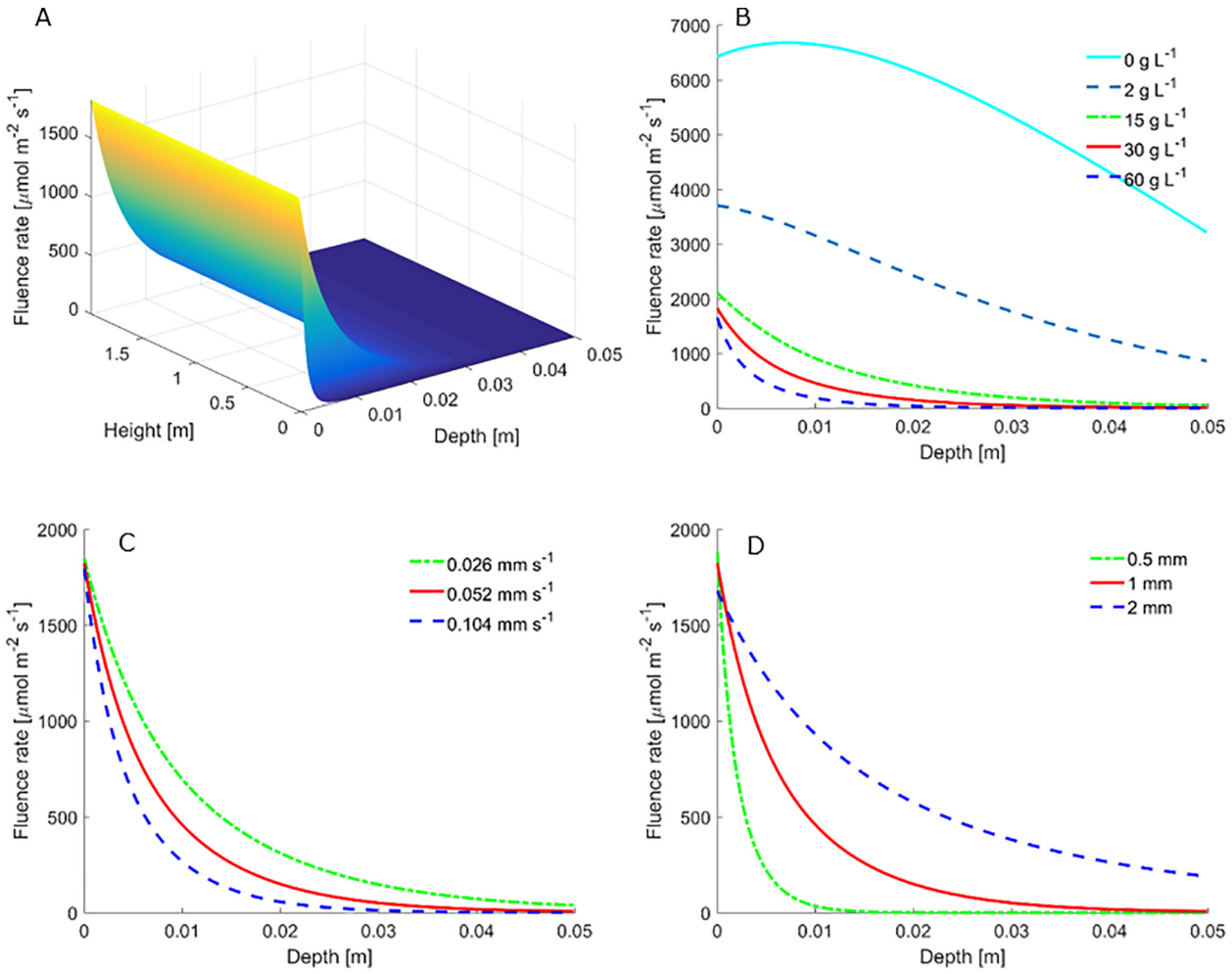

Fig. 7. Light distribution in the reactor, (a) presented as fluence rate as a function of depth and height, (b,c,d) presented as fluence rate at the mid-height of the reactor as a function of depth for (b) different C_x (c) different J_w (d) different r_b. For the simulation, the following inputs were applied unless otherwise indicated: r_b = 1 mm, J_G = 0.5 mm s^{-1}, J_w = 0.052 mm s^{-1}, E_o = 1500 μmol m^{-2} s^{-1}, C_x = 30 g L^{-1}, d = 5 cm, h = 2 m, assuming foam breaking at the top.

Table 2
Reflectance and transmittance values for a foam-bed containing varying C_x, and operating at different J_w and r_b. For the simulation, the following default inputs were applied: r_b = 1 mm, J_G = 0.5 mm s^{-1}, J_w = 0.052 mm s^{-1}, E_0 = 1500 μmol m^{-2} s^{-1}, C_x = 30 g L^{-1}, d = 5 cm, h = 2 m, assuming foam breaking at the top.

	C_x [g L^{-1}]					r_b [mm]			J_w [mm s^{-1}]		
	0	2	15	30	60	0.5	1	2	0.026	0.052	0.104
Reflectance [%]	61.0	30.1	12.0	8.8	6.8	9.4	8.8	7.1	9.0	8.8	8.4
Transmittance [%]	39.0	11.4	0.8	0.1	0.0	0.0	0.1	7.1	0.9	0.1	0.0

The high CO_2 uptake efficiency in a foam-bed photobioreactor is related to a high CO_2 transfer rate. The transfer rate can be described by the product of the volumetric mass transfer coefficient (k_La) and the driving force for mass transfer (the difference between the partial pressure of CO_2 in the gas and the liquid phases). The mean k_La value for CO_2 in our simulations is 0.045 s^{-1}, calculated as the multiplication of the liquid side mass transfer coefficient and the specific surface area, as explained in the Supplementary Information. Both k_L and a change over the foam column in height, but average values were calculated to be 1.54·10^{-5} m s^{-1} and 2923 m^{-1}, respectively. k_La values increase at reduced liquid fraction, due to the increased a and k_L values, therefore the lowest values are at the bottom of the foam-bed. The calculated k_L value is comparable to previously reported values in foam reactors of 3.10^{-5} m s^{-1}, and also the a value is comparable to reported values of 2150–3220 m^{-1} [16].

The specific surface area a was calculated assuming spherical bubbles. In case of reduced liquid fractions, the calculation of a therefore might be inaccurate due to bubble deformations [23], or due to unequal liquid distribution around the bubbles such as a reduced contribution of the thin liquid films [16,24]. Also a change in bubble size in height because of gas diffusion or coalescence/coarsening will lead to deviation of the specific surface area. When comparing the k_L values of a foam-bed bioreactor with those of conventional, liquid phase photobioreactors the k_L is lower in foam-bed reactors. This is related to reduce liquid flow and smaller gas bubbles in foam-bed photobioreactors [25]. The specific surface area a, on the other hand, is 60 times higher in a foam-bed photobioreactor. As a result, the k_La of 0.045 s^{-1} in the foam-bed photobioreactor is still 5 to 10 times higher compared to other systems: 0.007 or 0.009 s^{-1} was reported for a flat plate reactor [21,26], and 0.001–0.007 s^{-1} for bubble column photobioreactors

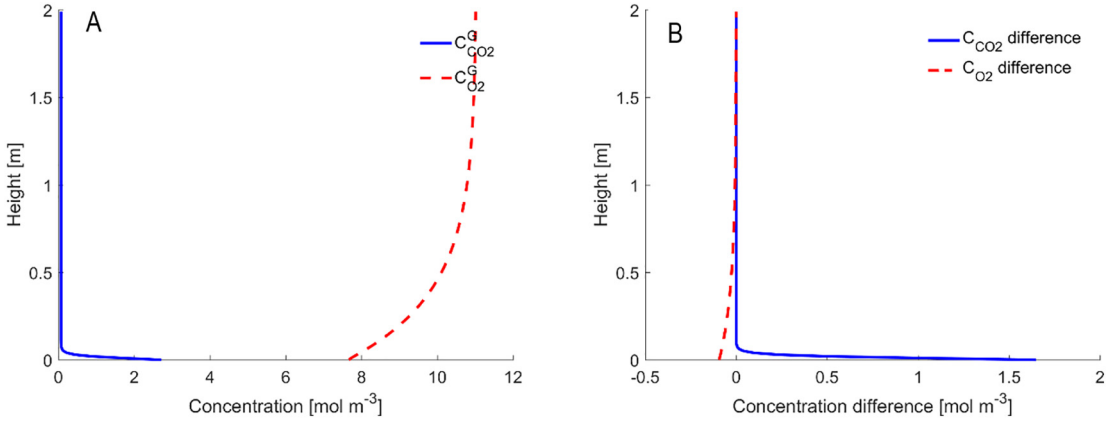

Fig. 8. A) O_2 and CO_2 concentration gradient in the gas phase. B) The driving force for mass transfer expressed as the concentration difference over the stationary liquid film surrounding the gas bubbles ($C_i^* - C_i^L$). Simulations were done at $C_x = 30\,g\,L^{-1}$, $r_b = 1\,mm$, $J_G = 0.5\,mm\,s^{-1}$, $E_0 = 1500\,\mu mol\,m^{-2}\,s^{-1}$, $d = 0.05\,m$, $h = 2\,m$. To convert from $mol\,m^{-3}$ to % of the compound in the gas phase, a factor of 2.5 can be used.

[27].

The majority of CO_2 transfer in the photobioreactor takes place at the bottom of the reactor, as illustrated in Fig. 8. Since the gas transfer rate in foam-bed photobioreactors is high, rapid CO_2 depletion takes place in the bubbles and therefore the liquid phase concentration increases quickly to the desired value ($5{\cdot}K_s$). This transferred CO_2 is used through the whole column for the algal growth, which is related to the assumption of an ideally mixed liquid phase. The decrease in the slope of the O_2 and CO_2 concentration in the gas phase is due to the decreased driving force for gas transfer in height due to the increasing O_2 and decreasing CO_2 concentrations at higher points in the reactor. In contrast to rapid CO_2 transfer, the O_2 concentration increases gradually in the column because of the reduced solubility of O_2, which is expressed by a higher Henry coefficient of O_2 than that of CO_2. The O_2 concentration difference over the thin liquid layer surrounding the gas bubbles is therefore reduced compared to that of CO_2 which therefore explains the different slopes of the driving force curve in height for the two gases (Fig. 8B).

Besides the sufficient CO_2 supply, also the O_2 concentrations in the liquid phase is relevant for photobioreactor designs. The tolerance of microalgae are estimated to be around 120–200% air saturation [28].However, most photobioreactors operate at severely increased O_2 concentrations up to several hundred percent air saturation [29,30]. In the simulated liquid foam-bed photobioreactor, the liquid O_2 concentration is 134% air saturation level, which is considered to be tolerable for the microalgae and therefore no inhibition effects are included.

4.4. Growth, productivity and energy requirement of a foam-bed photobioreactor

Light-dependent microalgal specific growth rate can be calculated based on the local fluence rate, which depends again on the biomass concentration as explained above. The productivity of the photobioreactor is the product of the biomass concentration and the average specific growth rate of the microalgae. The areal productivity of a conventional photobioreactor is thus mainly determined by the depth of the reactor and the biomass density maintained, which should be selected according to the illuminating light intensities. The light leaving the reactor should be minimal, but still allowing for the compensation for the maintenance requirements of the microalgal cells [31]. Too thin reactors in combination with low biomass densities lead to light losses, while too thick reactors result in a dark layer at the back of the reactor, where algal 'decay' takes place. Generally, in order to achieve a high biomass concentration, thin reactors are preferred [28], and there is an optimum biomass concentration where the reactor productivity is maximal [32]. In foam reactors, the liquid fraction of the foam plays an important role. Generally, foams consist of only < 10% liquid phase, and, as a result, in foam-bed photobioreactors biomass concentrations an order of magnitude higher than in conventional photobioreactors can be reached. This increase in biomass concentration of foam-beds is not entirely proportional to the decrease in light absorption path in foam-bed reactors compared to flat panels, since the light profile is altered due to scattering and some light is lost due to out-scattering of light from the photobioreactor as discussed before.

Besides reactor productivity, the energy invested for the production is a key factor when considering the feasibility of the system. The operational energy requirements for microalgae production in foam-bed photobioreactors depend on the energy requirements for gas supply and liquid circulations. In addition, the energy requirements for algal separation from a suspension is substantial and it scales inversely proportional to the biomass concentration.

The productivity and energy demand of a foam-bed photobioreactor is therefore highly dependent on the reactor design (dimensions of the system), light intensity, biomass concentration, and reactor operation (gas supply rate and liquid recirculation). It has to be noted that the biomass concentration is also an operational parameter as it can be controlled by reactor dilution. Also gas bubble size in the foam has significant effect on productivity by altering the light profile. For this reason, different conditions were evaluated by model simulations: incident light intensity, gas bubble size in the foam, superficial gas velocity, biomass concentration, and reactor depth. For each condition, the areal productivity shows a peak with varying liquid recirculation rates (Fig. 9), where the area refers to the illuminated reactor area. By adjusting the liquid recirculation rate for maximal productivity, the liquid fraction profile is altered to provide optimal light profiles, thus minimizing dark zones or unused light passing through the reactor. The biomass specific energy requirements are increasing with increased liquid recirculation rates, as a combined effect of increased energy for liquid recirculation and also for gas supply due to the increased hydrostatic pressure because of higher liquid fractions. Because of the dependence of the areal productivity on J_w, for further simulations at different conditions, the liquid recirculation rate was always optimized in order to achieve maximal areal biomass productivity.

Increasing the reactor height does not influence the areal productivities, since the liquid fraction is constant above the first few centimetres of the foam column. Consequently, higher reactors would not lead to further changes in the foam structure, leaving the growth rates unaltered in the vertical plane. The energy required for gas supply is also nearly proportional to the height (i.e. hydrostatic pressure), therefore the effect of height on reactor performance is negligible. The reactor height was arbitrarily fixed at 2 m.

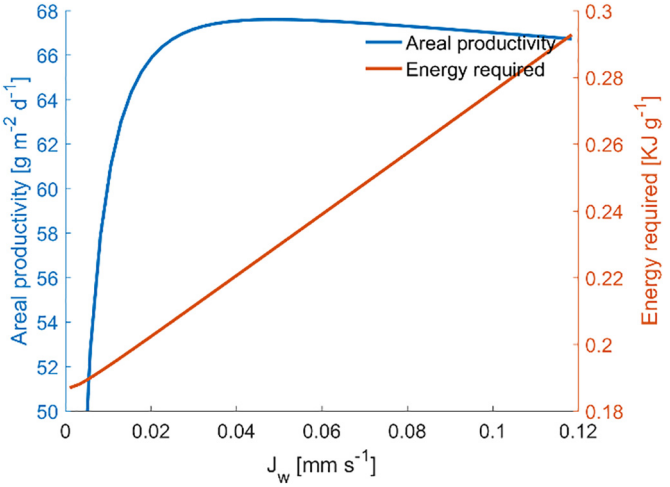

Fig. 9. Areal productivity and biomass specific energy requirements as a function of liquid recirculation rate, J_w under the default conditions of $C_x = 30\,g\,L^{-1}$, $r_b = 1\,mm$, $J_G = 0.5\,mm\,s^{-1}$, $E_0 = 1500\,\mu mol\,m^{-2}\,s^{-1}$, $d = 0.05\,m$, $h = 2\,m$.

When optimizing the superficial liquid recirculation rate J_w for maximal productivity, J_w increases from 0.01 to $4\,mm\,s^{-1}$ when the reactor depth decreases from 10 to 1 cm. Similarly, J_w increases from 0.02 to $0.12\,mm\,s^{-1}$ when the biomass concentration decreases from 60 to $15\,g\,L^{-1}$ (Table 3). A general trend can be observed: at higher biomass densities or in deeper reactors, the superficial liquid recirculation rate can be reduced. The resulting reduced liquid fraction allows for deeper light penetration in the reactor.

The minimal reactor depth applied, 1 cm, resulted in the highest areal productivity and photosynthetic efficiency (biomass yield on light). These values are $74.6\,g\,m^{-2}\,d^{-1}$ and $0.58\,g\,mol_{ph}{}^{-1}$, respectively (Table 3). However, the economic feasibility of such thin reactors are compromised due to the high energy requirements required for the liquid recirculation to reach a liquid fraction of 20%. Additionally, in thin reactors enhanced drainage is expected due to the increasing fraction of bubbles in contact with the walls, and therefore the calculated J_w might be underestimated [33]. In deeper reactors, not only the superficial recirculation rate, but also the total volumetric recirculation flow is reduced therefore the energy requirement for liquid recirculation decreases. Also, the reduced liquid fraction in deeper reactors result in reduced power for gas supply. Therefore, deep reactors are less energy-demanding, even when expressed as energy demand per g of biomass produced (calculations presented in the Supplementary Information). It has to be noted that in this study we focus on energy requirements corresponding to maximal areal productivities instead of minimizing biomass specific energy requirements. Minimal energy requirements are achieved under a lower liquid recirculation rate than obtained by optimizing for maximal areal productivity.

Amongst the three different biomass densities investigated (15, 30 and $60\,g\,L^{-1}$), $60\,g\,L^{-1}$ resulted in the highest areal productivity of $73.2\,g\,m^{-2}\,d^{-1}$ at $1500\,\mu mol\,m^{-2}\,s^{-1}$ in a 5 cm deep reactor. The reduced liquid fraction required for maximal productivity at $60\,g\,L^{-1}$ results in the reduction of scattering and therefore aids more advantageous light profiles. Besides, more absorbing media reduces the reflection as well, improving the biomass yield on light. Due to reduced liquid circulation and reduced harvest flow, the biomass specific energy requirements can be reduced from 0.49 to $0.11\,KJ\,g^{-1}$ when the biomass concentration is increased from 15 to $60\,g\,L^{-1}$.

At increased light intensities, higher liquid fractions are required in order to absorb most of the incoming light and prevent light leaving the system unused. On the one hand, the lowest incident light intensity ($375\,\mu mol\,m^{-2}\,s^{-1}$) results in the highest biomass yield on light, 0.88 g C_x $mol_{ph}{}^{-1}$, because the local fluence rates are around, or below, the saturation point of photosynthesis. On the other hand, the areal productivity is lowest at the lowest light intensity. When the recirculation rates are optimized in order to reach maximal areal productivity, the energy requirements are not significantly influenced by varying light intensities. This is reasoned by that at low intensities lower liquid fraction are optimal, and therefore reduced recirculation rates J_w have to be applied compared to higher light intensities with increased productivity.

The gas supply rate (J_G), the liquid recirculation rate (J_w), and the bubble size (r_b) together influence the liquid fraction of the foam and therefore the light distribution in the foam-bed photobioreactor, as shown in the previous section. Elevated liquid fraction and decreasing bubble size does not only increase the absorption coefficient of the foam, but also enhances the scattering. Therefore, the light profile is altered and it becomes steeper: the fluence rate decreases more rapidly with distance from the light exposed surface. A steeper light gradient is not beneficial since there is more photosaturation in the zone close to the light exposed surface while the light limited zone becomes larger. This results in a lower biomass yield on light and a decrease in areal productivity. The energy requirement in case of increased bubble size is higher since bigger bubbles imply reduced liquid fraction, and therefore an elevated recirculation rate has to be applied as compensation. The

Table 3
Simulation results of a mathematical model of a liquid foam-bed photobioreactor. The following parameters were calculated: Superficial liquid recirculation rate J_w, areal productivity r_x^{Areal}, biomass specific energy requirement E, and liquid fraction ε. The following parameters were varied: depth, biomass concentration, light intensity, gas flow rate and bubble radius. For each simulation the liquid recirculation value was optimized to obtain maximal areal productivity. Simulations were done at the following default values: $C_x = 30\,g\,L^{-1}$, $r_b = 1\,mm$, $J_G = 0.5\,mm\,s^{-1}$, $E_0 = 1500\,\mu mol\,m^{-2}\,s^{-1}$, $d = 0.05\,m$, $h = 2\,m$.

		J_w [$mm\,s^{-1}$]	r_x^{Areal} [$g\,m^{-2}\,d^{-1}$]	$Y_{x/ph}$ [$g\,mol_{ph}{}^{-1}$]	E [$KJ\,g^{-1}$]	ε [−]
Depth	1	4.00	74.6	0.58	0.79	0.20
d [cm]	5	0.05	67.6	0.52	0.23	0.03
	10	0.01	65.9	0.51	0.21	0.01
Biomass conc.	15	0.12	60.3	0.47	0.49	0.04
C_x [$g\,L^{-1}$]	30	0.05	67.6	0.52	0.23	0.03
	60	0.02	73.1	0.56	0.11	0.01
Light intensity	375	0.02	28.6	0.88	0.23	0.02
E_0 [$\mu mol\,m^{-2}\,s^{-1}$]	750	0.03	46.5	0.72	0.23	0.02
	1500	0.05	67.6	0.52	0.23	0.03
Superficial gas velocity	0.05	0.05	67.6	0.52	0.23	0.03
J_G [$mm\,s^{-1}$]	0.5	0.05	67.6	0.52	0.23	0.03
	2.5	0.03	67.6	0.52	0.24	0.03
Bubble radius	0.5	0.01	57.4	0.44	0.19	0.02
r_b [mm]	1	0.05	67.6	0.52	0.23	0.03
	2	0.27	74.5	0.57	0.39	0.03

energy required for bubble generation, however, is not taken into account. For example, > 5 times higher recirculation rate is required when the bubble size is increased from 1 to 2 mm, and consequently the energy requirements increase from 0.23 to 0.39 KJ g^{-1} (Table 3). Altered gas flow rates can also be compensated by adapting the liquid recirculation rate to maintain a constant liquid fraction and areal productivity. As such, a liquid fraction of 3% can be maintained. Reduced gas flow rates in combination with increased recirculation rates result in the lowest energy requirement, although the influence of gas flow rate on energy requirement is minimal (Table 3).

Altogether, these results and additional simulations of all conditions at 15 and 60 g L^{-1} show that the energy requirements are minimal at high biomass concentration and deep reactors (C_x = 60 g L^{-1}, E_0 = 1500 μmol m^{-2} s^{-1} and d = 10 cm, the E = 0.1 KJ g^{-1}). Since the highest areal productivities were achieved at 60 g L^{-1}, 1 cm depth and 1500 μmol m^{-2} s^{-1}, it is possible that the optimal areal productivity is still above this biomass concentration but was not studied in our simulations because of envisioned practical limitation, including: foam instability due to too high/low liquid fractions; physical-chemical changes in the liquid properties at C_x above 60 g L^{-1} [34], thereby influencing foaming properties; nutrient limitations in the liquid media. Additionally, high biomass concentrations might reduce the drainage rates due to confinement of the cells and their aggregates in the foam-bed, thereby reducing liquid recirculation requirements [35].

In a bench-scale liquid foam-bed photobioreactor, an areal productivity of 51.4 g m^{-2} d^{-1} was achieved, with a yield on light of 0.41 g mol_{ph}^{-1} at a biomass concentration of 6.81 g L^{-1}. These experiments were conducted with *Chlorella sorokiniana* in a circular foam column with a diameter of 10 cm, illuminated with a circular light source from all directions [8]. The experimentally achieved yield on light and areal productivities are 75–80% of the predicted ones for 30 g L^{-1} and 5 cm deep rectangular reactors. This difference is explained by suboptimal pH values and other non-optimized operational parameters. For example, the experimental recirculation rate was > 10 times higher than the one applied in the model, and also the experimental liquid dilution rate was 1.4 times higher compared to the model predictions. The experimentally obtained results therefore suggest that the model predictions are achievable when reactor operation is further optimized.

4.5. Foam-bed photobioreactors versus traditional photobioreactors

The potential of the foam-bed photobioreactors can be best evaluated when comparing them with existing photobioreactor types. In order to relate the performance of the foam-bed photobioreactor to traditional photobioreactors, their performance is simulated under the previously selected conditions: C_x = 30 g L^{-1}, d = 5 cm, h = 2 m, E_0 = 1500 μmol m^{-2} s^{-1}, J_w = 0.052 mm s^{-1}, J_G = 0.5 mm s^{-1}. The total biomass specific energy requirement for gas supply is 0.23 KJ g^{-1}, which consists of 8 J g^{-1} for gas supply, 43 J g^{-1} for liquid recirculation and 180 J g^{-1} for separation by a centrifuge.

The average growth rate μ^{av} in our simulations is 0.07 h^{-1}. A biomass volumetric productivity r_x of 53.3 g L_{liquid}^{-1} d^{-1} is achieved, which is significantly higher than values achieved in other short light path photobioreactors [36,37]. However, this increase is due to the low liquid content of the foam, and therefore the volumetric productivities calculated for the whole reactor are reduced by a factor equivalent to the liquid fraction of the foam. For a more fair comparison, the productivity per illuminated surface area was therefore calculated. An areal productivity of 67.7 g m^2 d^{-1} is predicted for the foam-bed photobioreactor, which is lower than areal productivities achieved in 14 mm light path reactors with *C. sorokiniana* under similar conditions. These productivities are 184.8 and 119 g m^{-2} d^{-1} under 2100 and 1500 μmol m^{-2} s^{-1}, respectively [36,37]. Since the reactor depth has a significant influence on areal productivity, flat panels and foam-bed reactors of the same depth can be compared. At a depth of 1 cm, the areal productivity of the foam-bed at a biomass concentration of 60 g L^{-1} is 3.06 g m^2 h^{-1}, approaching the areal productivity reported for flat panels, 3.89 g m^2 h^{-1} at 9.7 g L^{-1} biomass concentration [38].

The reason behind the lower areal productivities in a foam-bed photobioreactor is the reduced photosynthetic efficiency. Our simulations predicted 0.52 g biomass per mol of photons, which is lower compared to the ones achieved in flat panels, which range between 0.8 and 1 g mol_{ph}^{-1} [36,37,39]. The maximal theoretical yield of biomass on photons is 1.3 g biomass per mol photons calculated from our input parameters (Supplementary Information). The gap between the yield achieved experimentally in photobioreactors and the maximal theoretical yield lies in the horizontal light attenuation in the photobioreactors (photosaturation at the light exposed surface). The lower photosynthetic efficiency in the foam-bed compared to flat panels is due to light loss by reflection (9% of the incident light) and also due to a steeper and thus more unfavourable light gradient.

The energy requirement of microalgae production in a flat plate photobioreactor and in a foam-bed photobioreactor can be compared when the same microalgal species are used and the same light intensities applied. The operational energy requirement of flat panel photobioreactors is only determined by the gas supply. For our simulation, the energy requirement of a large-scale flat panel photobioreactor described by Ruiz et al. [2] was considered with the dimensions of 0.5 m height and 2 cm depth. In that study, a gassing rate of 0.32 vvm is described, translating to 0.0027 m s^{-1} superficial velocity. The biomass specific energy requirement was then calculated considering maximal productivities realized at lab-scale, 119 g m^{-2} d^{-1} achieved at 1500 μmol m^{-2} s^{-1} in a 14 mm light path reactor [37], in order to define an advantageous scenario for flat panels under continuous illumination. Finally, a biomass concentration of 2.3 g L^{-1} was assumed as described by Ruiz et al. [2] for 2 cm deep flat panels located in Curacao or Saudi Arabia. This biomass concentration is required in order to estimate the energy requirement for algae harvesting. According to these inputs, the biomass specific energy requirement for gas supply to flat panels is 0.38 KJ g^{-1} while the separation requires 2.35 KJ g^{-1}, resulting in a total biomass specific energy requirement of 2.73 KJ g^{-1}.

Foam-bed photobioreactors result in a decreased energy requirements for the gas supply. Reduction in energy takes place since the hydrostatic pressure exerted by the foam-bed is reduced by more than one order of magnitude compared to an equivalent water column and therefore less gas compression is required. In addition, the volumetric gas flow is reduced in foam-beds. Foam-bed photobioreactors require reduced superficial gas velocities compared to flat panels, since the gas transfer capacity is much higher due to the high interfacial area. In flat panel photobioreactors the k_La is highly dependent on J_G, high J_G values are required to achieve sufficient gas transfer [26]. However, in foam reactors applying liquid recirculation, an additional energy requirement for pumping liquid to the top of the reactor has to be considered. The energy requirement for the liquid recirculation is linearly related to the height of the photobioreactor and the liquid recirculation rate. The liquid pumps for the liquid recirculation require 5.3 times more energy compared to the gas supply to the foam-bed photobioreactor, therefore liquid recirculation is the major production-related operational energy requirement. Still, the total operational energy requirement of algal production in foam-bed photobioreactors are reduced compared to flat panels. For foam-beds, a power input to a reactor unit is 0.08 W, while for flat panels, 0.26 W is required.

The energy required for biomass separation is reduced in foam-bed photobioreactor compared to flat panels. The separation energy requirements are inversely related to the biomass concentration, therefore, an increase from 2.3 to 30 g L^{-1} results therefore in a proportional energy saving on separation. Thus, the energy required for biomass separation in foam-bed photobioreactors is 7.7% of that in flat panels. Since harvesting is more energy-demanding process compared to gas or liquid supply, (5.4 KJ L^{-1} of algal suspension) the biomass

concentration is critical for in the total energy requirement of the complete microalgae production process. Overall, the total production and harvesting energy requirements in the foam-bed photobioreactor are only 8.5% of flat panels (0.23 vs. 2.73 kJ g^{-1}).

5. Conclusions

A mathematical model was developed to evaluate the potential of liquid foam-bed photobioreactors. The model allowed simulation of the liquid fraction gradient, light penetration, microalgal growth, and gas transfer in foams under different conditions. Our simulations for the liquid fraction and the light profile were in a good agreement with experimental data. Model parametric sensitivity was studied for bubble radius, gas flow rate, liquid recirculation rate, light intensity, reactor depth, and biomass density. The model provided insight to the effect of the above listed parameters on areal productivity and energy requirements.

Our predictions at 30 g L^{-1} biomass and 1500 μmol m^{-2} s^{-1} resulted in a biomass yield on light of 0.52 g mol_{ph}^{-1} and an areal productivity of 67.7 g m^{-2} d^{-1}, while 0.23 KJ energy is required for the production of 1 g dry biomass. Although yield on light and areal productivity are lower than those in optimized flat panel photobioreactors, the energy demand is significantly lower in foam-bed photobioreactors. The lower biomass yield on light is related to light scattering in foams and thereby increasing light reflection and also resulting in a less advantageous light profile in foams. However, when practice allows, and cultivation at 60 g L^{-1} turns out to be feasible, these differences will be minimized. Moreover, the biomass specific energy requirement for microalgae production in foam-bed reactors is calculated to be only 8.5% of those in flat panels. These reduced energy requirements are due to a) increased biomass densities reducing the harvesting energy requirements; b) decreased gas supply due to increased gas transfer in foams (~6 times increased k_La) and decreased pressure of the foam column. In addition, the CO_2 uptake efficiency is severely improved and almost all CO_2 is taken up by the microalgal culture (97%). In conclusion, liquid foam-bed is a promising technology for microalgae cultivation.

Acknowledgements

This project has received funding from the European Union's Seventh Framework Programme for research, technological development and demonstration under grant agreement no 613588.

The authors would like to thank to Rob van der Vleugel for his work.

Declaration of authors contribution

Agnes Janoska is responsible for the integrity of the manuscript as a whole, conception and design, analysis and interpretation of the data and drafting of the article; Vasilis Andriopoulos is responsible for data acquisition; Rene H. Wijffels and Marcel Janssen are responsible for conception, design, critical revision of the article for important intellectual content and the final approval of the article.

Declarations of interest

None.

Statement of informed consent, human/animal rights

No conflicts, informed consent, human or animal rights applicable.

Appendix A. Parameter determination and model validation

A.1. Parameter determination

According to our experimental data, 10 CMC Pluronic F68 increased the viscosity of demineralised water with 11%, while the addition of microalgae (*Chlorella sorokiniana*) at a concentration of 5 g L^{-1} further increased the viscosity of the surfactant solution by 10% (total of 21% increase compared to demineralised water). The results are presented in Table A.1.

Table A.1
Dynamic viscosity of surfactant solution and inorganic media enriched with surfactant and microalgae.

Solution	Dynamic viscosity [mN s m^{-2}]
Demineralised water (value obtained from literature [40])	0.969
10 CMC pluronic F68 solution	1.0763
10 CMC pluronic F68 + 5 g L^{-1} microalgae solution	1.1755

The surface tension of M8a media, MilliQ water, microalgae solution, Pluronic F68 solution and the combination of surfactant and microalgae solution were measured, and the results are presented in Table A.2. The surface tension of a 10 CMC Pluronic F68 solution with microalgae (7.8 g L^{-1}) is 45 mN m^{-1}.

Table A.2
Surface tension of MilliQ water and inorganic media enriched with surfactant and/or microalgae.

Solution	Surface tension [mN m^{-1}]
MilliQ water	73.62
M8a media	72.33
7.8 g L^{-1} microalgae solution	63.06
10 CMC Pluronic F68	49.21
10 CMC Pluronic F68 + 7.8 g L^{-1} microalgae solution	44.95

Since the both viscosity and surface tension measurements were done at a 21.5 °C, thus a lower temperature than 37 °C used in the model, a factor for temperature correction was introduced based on the relative change in viscosity/surface tension of water between those temperatures [40], and those calculated values were applied in the model.

A.2. Validation of liquid fraction model

In order to validate the liquid fraction model, the average liquid fraction of the foam was experimentally determined and compared to the model outputs. The experimental conditions, including the measured bubble radius and liquid fraction values are presented in Table A.3. The increased bubble radius under conditions C and D compared to A and B are due to the elapsed time and consequent coalescence before the liquid addition is started, in order to create 'dry' foam.

When applying the measured r_b for the model simulations, the predicted liquid fraction is significantly higher than the experimental one. Comparable predictions to the experimental values can be achieved by applying increased bubble sizes for the model. This correction is reasoned since its well-known that bubble size measurements by image analysis of bubbles taken at the reactor wall are underestimating the real bubble sizes [41,42]. Also, the bubble sizes were measured at a certain height, and the further increase of the bubble size in height due to e.g. coarsening were not measured. This assumption is further supported by the observation of Yazhgur et al. [14], that the drainage model applied predicts the liquid fraction most accurate when instead of the mean radius, the radius corresponding to big bubbles are used, since big bubbles determine the foam permeability and govern the foam drainage. This remains true even if those big bubbles are rare.

With a factor of 2.3 to correct for the bubble size, the deviation in predicting the liquid fraction is always smaller than 10% for all different experimental conditions A–D (Table A.3). This correction factor was determined by minimizing the sum of the squares of the differences in liquid fraction between model and experiments. In the model simulations presented in the Manuscript and Supplementary Information, a fixed and homogenous bubble size of 1 mm was applied. These idealized model simulations are therefore not affected. When scaling up the foam-bed photobioreactor, however, preferably a foam-bed is created with homogenous bubbles size and/or the model predictions are improved by taking into account accurate bubble size distribution measurements.

Table A.3
Liquid fractions according to measurements (ε^m) and predictions ($\varepsilon^{Prediction}$) and the experimental conditions during the validation of the liquid fraction model. For each experimental condition, the listed variables which serve as inputs for the model predictions are height (h), superficial gas flow velocity (J_G), measured bubble radius r_b^m and superficial liquid addition rate (J_w). In the simulations for condition A and B, the liquid flux was calculated according to the theory of Yazhgur [14], since a rising foam was modelled, while for conditions C and D a standing foam with liquid addition was modelled, therefore the total liquid flux in the foam equals the extra liquid addition rate.

Condition	Liquid fraction		Experimental conditions					
	ε^m [%]	$\varepsilon^{Prediction}$ [%]	h [cm]	J_G [mm s^{-1}]	r_b^m [mm]	J_w [mm s^{-1}]	Surfactant concentration	J_f [mm s^{-1}]
A	11.06	10.75	20.79	3.46	0.168	0.00	10 CMC	calculated
B	8.09	8.79	14.15	2.36	0.168	0.00	5 CMC	calculated
C	3.83	4.2	20.79	0.00	0.378	0.092	10 CMC	$J_f = -J_w$
D	8.01	8.22	20.79	0.99	0.378	0.36	10 CMC	$J_f = -J_w$

A.3. Validation of light model

The light model was validated by measuring the fluence rate at several positions inside the foam-bed. In addition, the reflectance and transmittance was measured from the glass vessel filled with foam. Since the spherical light sensor (Walz US-SQS/A) measures fluence rate accurately only between −150° and + 150° incident angles because of a handlebar fixed on the sphere, a correction factor was introduced to recalculate the real fluence rate in a complete isotropic light field from the measured value. This factor was calculated to be 1.3 based on the angular distribution of the fluence rate measured by the sensor which was provided by Walz (Walz Gmbh, Germany).

The fluence rate inside the foam is plotted in Fig. A.1 for 5 different depths with 475 µmol m^{-2} s^{-1} incident irradiance. In most cases, the corrected fluence rate is closer to the model predictions, indicating that the assumption of isotropic light is not incorrect. Predicted fluence rates and reflectance/transmittance values show some deviations from the experimental values in the different cases with different biomass concentrations.

The prediction of fluence rate in non-absorbing, clear foam is slightly higher compared to the measured and corrected value. This might be due to light escaping also at the sides of the glass container, therefore reducing the experimental fluence rate. The sum of the measured transmittance and reflectance in non-absorbing foams are over 100%, possibly due to the inaccuracy in reflectance measurements. An error in the light reflection measurements is more likely since the measurement point was further from the glass vessel, and therefore light spreading took place. This was corrected by the fraction of light that arrives to the measurement point when a white and black paper sheet was applied instead of the foam vessel. The white surface is assumed to represent complete diffuse reflectance while the black surface represents complete absorbance. Therefore, these measurements depend on many parameters, such as the absorption and reflection from the paper sheets and the angular distributions of reflections from both the foam and the white paper. As expected, for the model simulations the sum of reflection and transmission is 100% and the light balance closes. Considering the measurement error in the reflectance measurements, the model predicts the light distribution well.

In foam with increasing microalgae concentration, the simulations predict a steeper decrease of fluence rate with depth compared to the measurements (Fig. 3B, C and D). The reflectance and transmittance values are systematically underestimated by the model compared to the measured values. It is unsure whether the deviations are due to the inaccuracy in the measurements, since the light balance does not close, or are related to an incomplete model description. In the model, the absorption cross section of a photoacclimated microalgal mass culture was applied, which does not necessarily represent the absorption cross section of the culture used in the experiments. In addition, the measured reflectance might have been overestimated because the white paper sheets (3 sheets of 80 g m^{-2}) do not represent total reflectance, as the corresponding albedo is below 1. Also, inaccuracies in bubble size measurements or inhomogeneous liquid supply from the top might result in an altered liquid fraction, leading to different reflectance/transmittance.

The light model outputs, such as, reflectance, transmittance and fluence rate profile in depth show the same pattern as the measured values. These patterns include the reflectance and transmittance decrease with increasing biomass concentration and also the increase of local fluence rate at the front of the reactor (up to 5 times the irradiance) and its consequent decrease in depth due to absorption and scattering. Therefore, in terms of the

most important characteristics of light transport, good predictions are obtained.

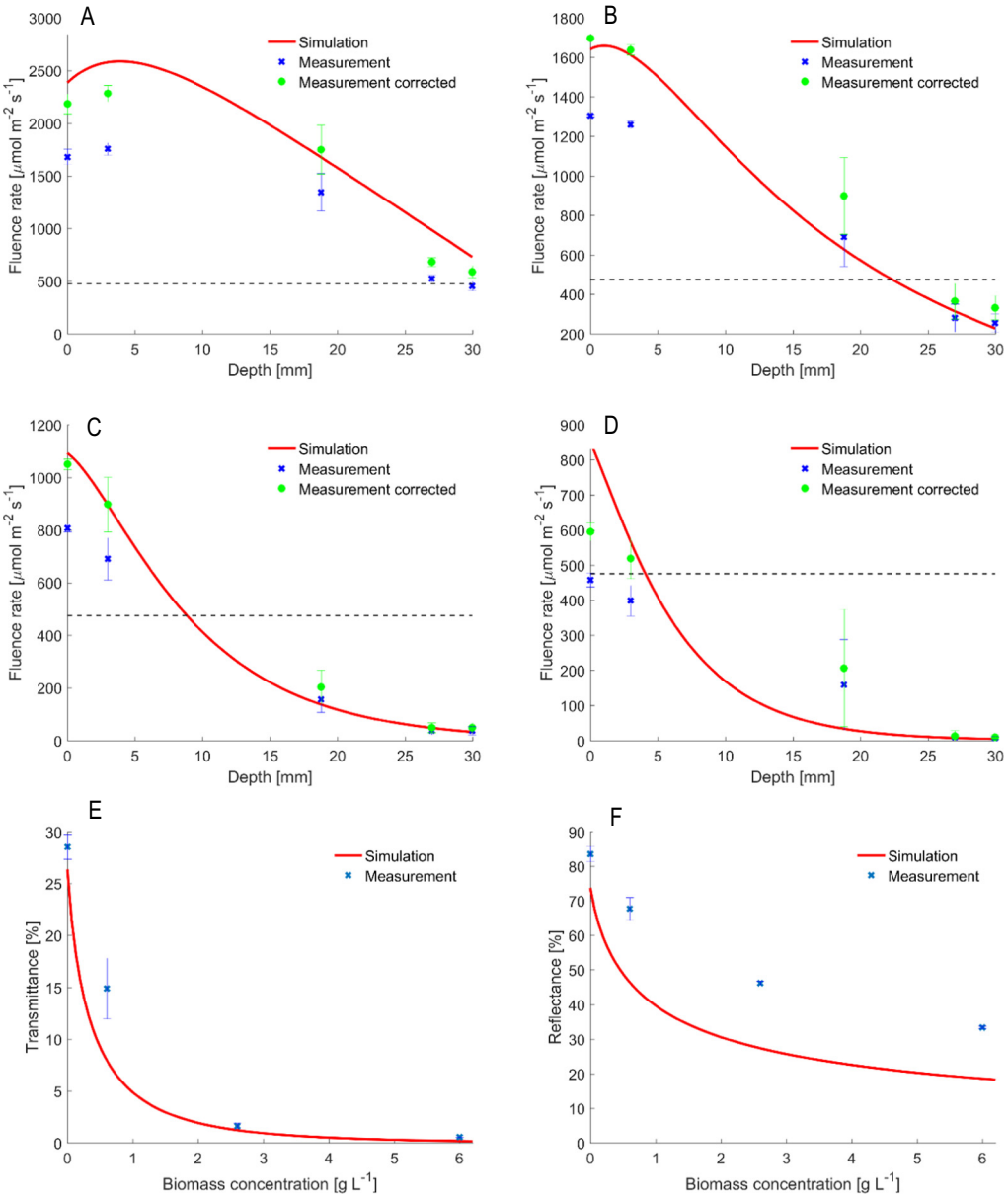

Fig. A.1. Light validation experiments and corresponding model simulations: A) Clear foam; B) 0.6 g L^{-1} microalgae concertation C) 2.6 g L^{-1} microalgae concentration D) 6 g L^{-1} microalgae concentration. The horizontal dashed line indicates the incident light intensity. E) represents the transmittance and F) the reflectance from the glass container.

Appendix B. Supplementary data

The detailed model description is presented as Supplementary Information. In this file, the inputs, variables and parameters are applied in the model are listed, and the equations corresponding to the liquid fraction gradient in height, light penetration, mass transfer, algal growth and energy requirements of the liquid foam-bed photobioreactor are presented. Supplementary data to this article can be found online at https://doi.org/10.1016/j.algal.2018.09.029.

References

[1] R.H. Wijffels, M.J. Barbosa, M.H. Eppink, Microalgae for the production of bulk chemicals and biofuels, Biofuels Bioprod. Biorefin. 4 (2010) 287–295.
[2] J. Ruiz, G. Olivieri, J. de Vree, R. Bosma, P. Willems, J.H. Reith, M.H. Eppink, D.M. Kleinegris, R.H. Wijffels, M.J. Barbosa, Towards industrial products from microalgae, Energy Environ. Sci. 9 (2016) 3036–3043.
[3] R.N. Singh, S. Sharma, Development of suitable photobioreactor for algae production – a review, Renew. Sust. Energ. Rev. 16 (2012) 2347–2353.
[4] A. Janoska, P.P. Lamers, A. Hamhuis, Y. van Eimeren, R.H. Wijffels, M. Janssen, A liquid foam-bed photobioreactor for microalgae production, Chem. Eng. J. 313 (2017) 1206–1214.
[5] P. Stevenson, Hydrodynamic theory of rising foam, Miner. Eng. 20 (2007) 282–289.
[6] N. Isert, G. Maret, C.M. Aegerter, Coarsening dynamics of three-dimensional levitated foams: from wet to dry, Eur. Phys. J. E 36 (2013) 116–121.
[7] A.-L. Biance, A. Delbos, O. Pitois, How topological rearrangements and liquid fraction control liquid foam stability, Phys. Rev. Lett. 106 (2011) 068301.
[8] A. Janoska, R. Barten, S. de Nooy, P. van Rijssel, René H. Wijffels, M. Janssen, Improved liquid foam-bed photobioreactor design for microalgae cultivation, Algal Res. 33 (2018) 55–70.
[9] A. Janoska, M. Vázquez, M. Janssen, R.H. Wijffels, M. Cuaresma, C. Vílchez,

Surfactant selection for a liquid foam-bed photobioreactor, Biotechnol. Prog. (2018), https://doi.org/10.1002/btpr.2614.
[10] W. Blanken, P.R. Postma, L. de Winter, R.H. Wijffels, M. Janssen, Predicting microalgae growth, Algal Res. 14 (2016) 28–38.
[11] R. Kant Sharma, A. Gaikwad, A.N. Bhaskarwar, Gas absorption with chemical reaction and desorption in a foam-bed reactor, Chem. Eng. Commun. 192 (2005) 597–619.
[12] E. Kan, M.A. Deshusses, Modeling of a foamed emulsion bioreactor: I. model development and experimental validation, Biotechnol. Bioeng. 99 (2008) 1096–1106.
[13] P. Ireland, R. Cunningham, G.J. Jameson, The behaviour of wash water injected into a froth, Int. J. Miner. Process. 84 (2007) 99–107.
[14] P. Yazhgur, E. Rio, F. Rouyer, F. Pigeonneau, A. Salonen, Drainage in a rising foam, Soft Matter 12 (2016) 905–913.
[15] A.J. Welch, M.J. Van Gemert (Eds.), Optical-thermal response of laser-irradiated tissue, second ed., Springer, Dordrecht, 2011.
[16] D.C. Perry, P. Stevenson, Gas absorption and reaction in a wet pneumatic foam, Chem. Eng. Sci. 126 (2015) 177–185.
[17] A.M. Kliphuis, D.E. Martens, M. Janssen, R.H. Wijffels, Effect of O_2:CO_2 ratio on the primary metabolism of *Chlamydomonas reinhardtii*, Biotechnol. Bioeng. 108 (2011) 2390–2402.
[18] S.M. Walas, Chemical Process Equipment-Selection and Design, Butterworth-Heinemann, USA, 1990.
[19] J. Doucha, K. Lívanský, Novel outdoor thin-layer high density microalgal culture system: productivity and operational parameters, Algol. Stud. Supplement 76 (1995) 129–147.
[20] J. Doucha, F. Straka, K. Lívanský, Utilization of flue gas for cultivation of microalgae (*Chlorella* sp.) in an outdoor open thin-layer photobioreactor, J. Appl. Phycol. 17 (2005) 403–412.
[21] R. Reyna-Velarde, E. Cristiani-Urbina, D.J. Hernández-Melchor, F. Thalasso, R.O. Cañizares-Villanueva, Hydrodynamic and mass transfer characterization of a flat-panel airlift photobioreactor with high light path, Chem. Eng. Process. Process Intensif. 49 (2010) 97–103.
[22] T.M. Sobczuk, F.G. Camacho, F.C. Rubio, F. Fernandez, E.M. Grima, Carbon dioxide uptake efficiency by outdoor microalgal cultures in tubular airlift photobioreactors, Biotechnol. Bioeng. 67 (2000) 465–475.
[23] R. Höhler, Y. Yip Cheung Sang, E. Lorenceau, S. Cohen-Addad, Osmotic pressure and structures of monodisperse ordered foam, Langmuir 24 (2008) 418–425.
[24] O. Pitois, E. Lorenceau, N. Louvet, F. Rouyer, Specific surface area model for foam permeability, Langmuir 25 (2008) 97–100.
[25] M. Bouaifi, G. Hebrard, D. Bastoul, M. Roustan, A comparative study of gas hold-up, bubble size, interfacial area and mass transfer coefficients in stirred gas–liquid reactors and bubble columns, Chem. Eng. Process. Process Intensif. 40 (2001) 97–111.
[26] E. Sierra, F.G. Acién, J.M. Fernández, J.L. García, C. González, E. Molina, Characterization of a flat plate photobioreactor for the production of microalgae, Chem. Eng. J. 138 (2008) 136–147.
[27] C.J. Hulatt, D.N. Thomas, Productivity, carbon dioxide uptake and net energy return of microalgal bubble column photobioreactors, Bioresour. Technol. 102 (2011) 5775–5787.
[28] C. Posten, Design principles of photo-bioreactors for cultivation of microalgae, Eng. Life Sci. 9 (2009) 165–177.
[29] E. Molina, J. Fernández, F. Acién, Y. Chisti, Tubular photobioreactor design for algal cultures, J. Biotechnol. 92 (2001) 113–131.
[30] J.C. Weissman, R.P. Goebel, J.R. Benemann, Photobioreactor design: mixing, carbon utilization, and oxygen accumulation, Biotechnol. Bioeng. 31 (1988) 336–344.
[31] H. Takache, G. Christophe, J.F. Cornet, J. Pruvost, Experimental and theoretical assessment of maximum productivities for the microalgae *Chlamydomonas reinhardtii* in two different geometries of photobioreactors, Biotechnol. Prog. 26 (2010) 431–440.
[32] H. Qiang, A. Richmond, Productivity and photosynthetic efficiency of *Spirulina platensis* as affected by light intensity, algal density and rate of mixing in a flat plate photobioreactor, J. Appl. Phycol. 8 (1996) 139–145.
[33] S.A. Koehler, S. Hilgenfeldt, H. Stone, Foam drainage on the microscale: I. Modeling flow through single plateau borders, J. Colloid Interface Sci. 276 (2004) 420–438.
[34] A. Wileman, A. Ozkan, H. Berberoglu, Rheological properties of algae slurries for minimizing harvesting energy requirements in biofuel production, Bioresour. Technol. 104 (2012) 432–439.
[35] B. Haffner, Y. Khidas, O. Pitois, The drainage of foamy granular suspensions, J. Colloid Interface Sci. 458 (2015) 200–208.
[36] M. Cuaresma, M. Janssen, C. Vílchez, R.H. Wijffels, Productivity of *Chlorella sorokiniana* in a short light-path (SLP) panel photobioreactor under high irradiance, Biotechnol. Bioeng. 104 (2009) 352–359.
[37] T. de Mooij, Z.R. Nejad, L. van Buren, R.H. Wijffels, M. Janssen, Effect of photoacclimation on microalgae mass culture productivity, Algal Res. 22 (2017) 56–67.
[38] K. Tuantet, H. Temmink, G. Zeeman, M. Janssen, R.H. Wijffels, C.J. Buisman, Nutrient removal and microalgal biomass production on urine in a short light-path photobioreactor, Water Res. 55 (2014) 162–174.
[39] A.M. Kliphuis, L. de Winter, C. Vejrazka, D.E. Martens, M. Janssen, R.H. Wijffels, Photosynthetic efficiency of *Chlorella sorokiniana* in a turbulently mixed short light-path photobioreactor, Biotechnol. Prog. 26 (2010) 687–696.
[40] University of Reading, Calculator to estimate the density and viscosity of glycerine/water mixtures, http://www.met.reading.ac.uk/~sws04cdw/viscosity_calc.html, (2017) , Accessed date: 30 January 2018.
[41] H.C. Cheng, R. Lemlich, Errors in the measurement of bubble size distribution in foam, Ind. Eng. Chem. Fundam. 22 (1983) 105–109.
[42] R. Shaw, G.M. Evans, P. Stevenson, Start-up transients in a pneumatic foam, Asia Pac. J. Chem. Eng. 6 (2011) 613–623.